Automated Pericardial Fat Quantification from Coronary Magnetic Resonance Angiography

Xiaowei Ding[12]
xiaowei@cs.ucla.edu
Jianing Pang[1]
Jianing.Pang@cshs.org
Zhou Ren[2]
zhou.ren@cs.ucla.edu
Mariana Diaz-Zamudio[3]
diazzmariana@gmail.com
Daniel S Berman[34]
Daniel.Berman@cshs.org
Debiao Li[14]
Debiao.Li@cshs.org
Demetri Terzopoulos[2]
dt@cs.ucla.edu
Piotr J. Slomka[34]
Piotr.Slomka@cshs.org
Damini Dey[14]
Damini.Dey@cshs.org

[1] Biomedical Imaging Research Institute, Department of Biomedical Sciences, Cedars Sinai Medical Center, Los Angeles, CA, USA

[2] Computer Science Department, Henry Samueli School of Engineering and Applied Science at UCLA, Los Angeles, CA USA

[3] Departments of Imaging and Medicine, Cedars Sinai Medical Center, Los Angeles, CA, USA

[4] Department of Medicine, David-Geffen School of Medicine at UCLA, Los Angeles, CA, USA

Abstract

Pericardial fat volume (PFV) is emerging as an important parameter for cardiovascular risk stratification. We propose a hybrid multi-atlas and graph-based segmentation approach for automated PFV quantification from water/fat-resolved whole-heart "needle-free" non-contrast coronary magnetic resonance angiography (MRA). We validated the quantification results on 6 subjects and compared them with manual quantifications by an expert reader. The PFV quantified by our algorithm was 62.78 ± 27.85 cm^3 compared to 58.66 ± 27.05 cm^3 by the expert, which were not significantly different ($p = 0.47$, mean percent difference $9.6 \pm 9.5\%$) and showed excellent correlation ($R = 0.89$, $p < 0.01$). The mean Dice coefficient of pericardial fat voxels was 0.82 ± 0.06 (median 0.85). Using our approach, physicians can accurately quantify patients' pericardial fat volume from MRI without tedious manual tracing. To our knowledge, this is the first report of an automated algorithm for PFV from whole-heart, non-contrast coronary MRA images.

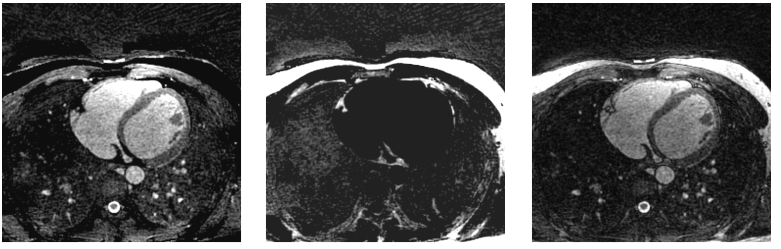

(a) water-only image (b) fat-only image (c) water-fat fused image

Figure 1: Example transverse slices of MRA data.

1 Introduction

Recent studies have shown that pericardial fat is strongly associated with coronary artery disease (CAD), coronary calcium scores (CCS), severity of detected CAD, biochemical markers of systemic inflammation, risk of future adverse cardiovascular events, and myocardial ischemia [1, 2, 3, 4, 5, 7, 10, 13, 14].

Most pericardial fat studies and quantification algorithm development were done on CT data [1, 2, 3, 4, 5, 7, 10, 13, 14]. However, MRI imposes no ionizing radiation on patients and can also separate fat and non-fat tissues from the signal. To date, pericardial fat quantification in MRI was reported on manually outlined regions of interest (ROI), which are subject to inter-observer and inter-scan variability. Miao [11] and Wong [15] used manual tracing tools to quantify pericardial fat on MRI. Thus, it is highly desirable to develop an automated algorithm that provides fast and consistent results with minimal human intervention and few labeled datasets.

In this paper, we propose an algorithm for automated pericardial fat quantification from water/fat-resolved whole-heart coronary magnetic resonance angiography (MRA). The algorithm fuses the advantages of multi-atlas-based segmentation [2, 9] and graph-based segmentation [6] to achieve voxel-level segmentation accuracy. The algorithm first roughly segments the heart region using a simplified atlas-based segmentation on the fat-water fused image. The multi-atlas is created using a small number of labeled datasets (4 subjects) with expert manual 3D masks of the heart region. To get exact boundaries of pericardial fat and minimize the risk of incorrect quantification caused by the errors introduced from the atlas segmentation, a 3D graph-based segmentation is used to generate fat and non-fat components on the fat-only image. The algorithm then selects the components that represent pericardial fat using intensity features and their relative positions with the heart region.

2 Materials and Methods

MR data were collected on a clinical 1.5 Tesla scanner (MAGNETOM Avanto, Siemens AG Healthcare, Erlangen, Germany) using a free-breathing, electro-cardiograph-gated, balanced steady-state free-precession pulse sequence with 3D radial k-space trajectory and retrospective, image-based respiratory motion correction. Matrix size = $384 \times 384 \times 384$, voxel size = $1mm \times 1mm \times 1mm$. Water-only $I_w(\mathbf{p})$ and fat-only $I_f(\mathbf{p})$ images were calculated based on the pixel-by-pixel complex phase of the raw image [8]. More details of the MR acquisition and reconstruction framework can be found in previous works by Pang et al.[12].

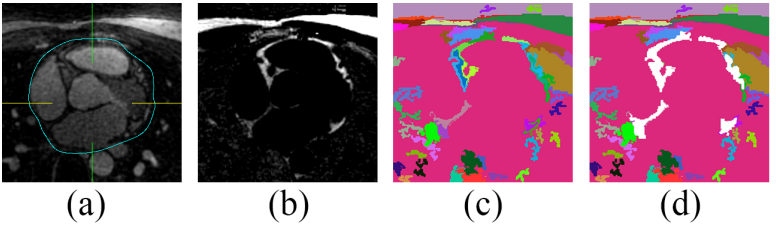

Figure 2: Main steps of our algorithm. (a) Multi-atlas-based segmentation of the heart region. (b) Perform 3D graph-based segmentation on fat-only image. Colors are representation of different components. (c) Fat components and non-fat components. (d) Pericardial fat component selection (white components).

On the basis of multi-atlas-based segmentation and efficient graph-based segmentation, we propose a quantification technique divided into two steps. First, the heart region initialization is performed using a simplified multi-atlas segmentation with local decision fusion [9] on water-fat fused images (Figure 2(a)). Voxels are over-segmented into components on fat-only images using an efficient graph-based segmentation method [6] (Figure 2(b)(c)), which we generalized from 2D space to 3D space in this work. The fat components with certain intensity features and overlap rate with the heart region masks are selected as pericardial fat (Figure 2(d)).

2.1 Simplified multi-atlas-based heart region segmentation

The multi-atlas segmentation determines the initial location and shape of the heart. The atlas was created from multiple subject scans (water-fat fused images) with wide BMI range (N = 4; 2 men and 2 women, BMI 17, 22, 28, 35). For the atlas creation, on all transverse slices, 2D pericardial contours were manually traced by an expert cardiologist physician within the superior and inferior limits of the heart. A 3D binary volume mask was generated from the 2D contours. Target image segmentation was achieved by one-to-all image registration between the target image and atlas images[9].

The results of multi-atlas segmentation provide global localization of the heart region with limited accuracy at the boundaries of the pericardial fat due to the global registration scheme and the small atlas. The next graph-based segmentation step can generate the exact boundaries of the pericardial fat.

2.2 3D graph-based fat component segmentation and selection

We construct a fully-connected undirected 3D graph $G = (V,E)$ on the 3D fat-only image $I_f(\mathbf{p})$ with vertices $v_i \in V$ located on each voxel, and edges $(v_i, v_j) \in E$ corresponding to pairs of neighboring vertices. Each edge $(v_i, v_j) \in E$ has a corresponding weight $w((v_i, v_j))$, which is a non-negative measure of the dissimilarity between neighboring elements v_i and v_j. A segmentation S is a partition of V into components such that each component $C \in S$ corresponds to a connected component in a graph $G' = (V,E')$. The algorithm starts with initial segmentation S_{init} where each vertex v_i is in its own component.

In this formulation, we want the voxels in a component to be similar and voxels in different components to be dissimilar; i.e., to have either fat voxels or non-fat voxels in one

component. We define a predicate D based on [6] for evaluating whether or not there is evidence for the boundary between two components in a segmentation. The predicate compares the inter-component differences to the within-component differences and is thereby adaptive with respect to the local characteristics of the data, hence dealing with intensity variation and noise in the MRA image.

The *internal difference* of a component $C \subseteq V$ is defined as

$$\mathrm{Int}(C) = \max_{e \in MST(C,E)} w(e), \tag{1}$$

the largest weight in the minimum spanning tree $MST(C,E)$ of the component. The *difference between two components* $C_1, C_2 \subseteq V$ is defined as the minimum weight edge connecting the two components:

$$\mathrm{Diff}(C_1,C_2) = \min_{v_i \in C_1, v_j \in C_2, (v_i,v_j) \in E} w((v_i,v_j)). \tag{2}$$

If there is no edge connecting C_1 and C_2, we let $\mathrm{Diff}(C_1,C_2) = \infty$. The pairwise comparison predicate is

$$D(C_1,C_2) = \begin{cases} true & if \quad \mathrm{Diff}(C_1,C_2) > \mathrm{MInt}(C_1,C_2), \\ false & otherwise, \end{cases} \tag{3}$$

where the minimum internal difference MInt is defined as

$$\mathrm{MInt}(C_1,C_2) = \min\left(\mathrm{Int}(C_1) + k/|C_1|,\ \mathrm{Int}(C_2) + k/|C_2|\right), \tag{4}$$

where $|C|$ denotes the size of C and k is a constant parameter which sets a scale of observation. A larger k causes a preference for larger components, but k is not a minimum component size.

After we obtain all the 3D segment components C_i (Figure 2(c)) using the iterative algorithm in [6], the mean intensity of each components t_i and overlap rate o_i with the heart region from last step are calculated. Components C_i with $t_i > T$ and $o_i > O$ are selected as pericardial fat components (Figure 2(d)), where T and O are threshold values for component mean intensity and overlap rate, respectively, with the heart region masks. The pericardial fat volume can be calculated by multiplying the total number of pericardial fat voxels by the voxel size.

3 Results

We performed the MRA scan described in Section 2 on 10 subjects of which 4 were used to create the atlas, with the remaining 6 used for testing.

The pericardial fat volume for the 6 test datasets was quantified as 62.78 ± 27.85 cm^3 by our automated algorithm and 58.66 ± 27.05 cm^3 according to the expert manual quantification, with no significant difference ($p = 0.47$, mean percent difference $9.6 \pm 9.5\%$) and excellent correlation ($R = 0.89$, $p < 0.01$). The mean Dice coefficient of pericardial fat voxels was 0.82 ± 0.06 (median 0.85). An example comparing algorithm segmentation and manual segmentation results is shown in figure 3.

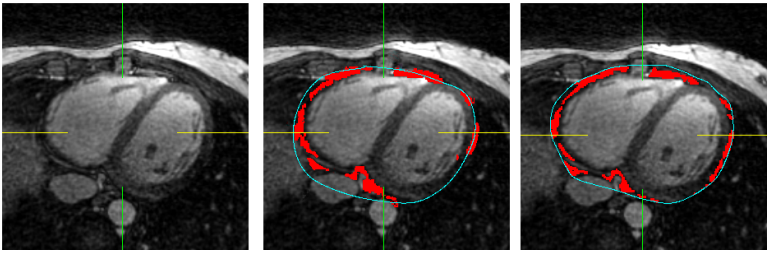

Figure 3: Example comparing algorithm segmentation and manual segmentation results. The red overlays represent pericardial voxels and the blue contours represent heart region boundaries.

4 Conclusion

The quantification of pericardial fat volume from "needle-free" non-contrast MRA is feasible via a hybrid approach using multi-atlas-based heart region initialization and the 3D graph-based segmentation and selection of pericardial fat components. Our preliminary results demonstrate that physicians can accurately quantify patients' pericardial fat volume from "needle-free" non-contrast MRA without tedious manual tracing.

References

[1] Victor Y Cheng, Damini Dey, Balaji Tamarappoo, Ryo Nakazato, Heidi Gransar, Romalisa Miranda-Peats, Amit Ramesh, Nathan D Wong, Leslee J Shaw, Piotr J Slomka, et al. Pericardial fat burden on ECG-gated noncontrast CT in asymptomatic patients who subsequently experience adverse cardiovascular events. *JACC: Cardiovascular Imaging*, 3(4):352–360, 2010.

[2] Damini Dey, Amit Ramesh, Piotr J Slomka, Ryo Nakazato, Victor Y Cheng, Guido Germano, and Daniel S Berman. Automated algorithm for atlas-based segmentation of the heart and pericardium from non-contrast CT. In *SPIE Medical Imaging*, pages 762337–762337. International Society for Optics and Photonics, 2010.

[3] Damini Dey, Nathan D Wong, Balaji Tamarappoo, Ryo Nakazato, Heidi Gransar, Victor Y Cheng, Amit Ramesh, Ioannis Kakadiaris, Guido Germano, Piotr J Slomka, et al. Computer-aided non-contrast CT-based quantification of pericardial and thoracic fat and their associations with coronary calcium and metabolic syndrome. *Atherosclerosis*, 209(1):136–141, 2010.

[4] Jingzhong Ding, Stephen B Kritchevsky, Tamara B Harris, Gregory L Burke, Robert C Detrano, Moyses Szklo, and J Jeffrey Carr. The association of pericardial fat with calcified coronary plaque. *Obesity*, 16(8):1914–1919, 2008.

[5] Xiaowei Ding, Demetri Terzopoulos, Mariana Diaz-Zamudio, Daniel S Berman, Piotr J Slomka, and Damini Dey. Automated epicardial fat volume quantification from non-

contrast CT. In *SPIE Medical Imaging*, pages 90340I–90340I. International Society for Optics and Photonics, 2014.

[6] Pedro F Felzenszwalb and Daniel P Huttenlocher. Efficient graph-based image segmentation. *International Journal of Computer Vision*, 59(2):167–181, 2004.

[7] Martin Greif, Alexander Becker, Franz von Ziegler, Corinna Lebherz, Michael Lehrke, Uli C Broedl, Janine Tittus, Klaus Parhofer, Christoph Becker, Maximilian Reiser, et al. Pericardial adipose tissue determined by dual source CT is a risk factor for coronary atherosclerosis. *Arteriosclerosis, Thrombosis, and Vascular Biology*, 29(5):781–786, 2009.

[8] Brian A Hargreaves, Shreyas S Vasanawala, Krishna S Nayak, Bob S Hu, and Dwight G Nishimura. Fat-suppressed steady-state free precession imaging using phase detection. *Magnetic Resonance in Medicine*, 50(1):210–213, 2003.

[9] Ivana Isgum, Marius Staring, Annemarieke Rutten, Mathias Prokop, Max A Viergever, and Bram van Ginneken. Multi-atlas-based segmentation with local decision fusion: Application to cardiac and aortic segmentation in CT scans. *Medical Imaging, IEEE Transactions on*, 28(7):1000–1010, 2009.

[10] Amir A Mahabadi, Joseph M Massaro, Guido A Rosito, Daniel Levy, Joanne M Murabito, Philip A Wolf, Christopher J O'Donnell, Caroline S Fox, and Udo Hoffmann. Association of pericardial fat, intrathoracic fat, and visceral abdominal fat with cardiovascular disease burden: The framingham heart study. *European Heart Journal*, 30(7): 850–856, 2009.

[11] Cuilian Miao, Shaoguang Chen, Jingzhong Ding, Kiang Liu, Debiao Li, Robson Macedo, Shenghan Lai, Jens Vogel-Claussen, Elizabeth R Brown, Jo?? o AC Lima, et al. The association of pericardial fat with coronary artery plaque index at MR imaging: The multi-ethnic study of atherosclerosis (mesa). *Radiology*, 261(1):109–115, 2011.

[12] Jianing Pang, Behzad Sharif, Reza Arsanjani, Xiaoming Bi, Zhaoyang Fan, Qi Yang, Kuncheng Li, Daniel S Berman, and Debiao Li. Accelerated whole-heart coronary MRA using motion-corrected sensitivity encoding with three-dimensional projection reconstruction. *Magnetic Resonance in Medicine*, 73(1):284–291, 2015.

[13] Sanjay Sarin, Christopher Wenger, Ajay Marwaha, Anwer Qureshi, Bernard DM Go, Cathleen A Woomert, Karla Clark, Louis A Nassef, and Jamshid Shirani. Clinical significance of epicardial fat measured using cardiac multislice computed tomography. *The American Journal of Cardiology*, 102(6):767–771, 2008.

[14] Rie Taguchi, Junichiro Takasu, Yasutaka Itani, Rie Yamamoto, Kenichi Yokoyama, Shigeru Watanabe, and Yoshiaki Masuda. Pericardial fat accumulation in men as a risk factor for coronary artery disease. *Atherosclerosis*, 157(1):203–209, 2001.

[15] Christopher X Wong, Hany S Abed, Payman Molaee, Adam J Nelson, Anthony G Brooks, Gautam Sharma, Darryl P Leong, Dennis H Lau, Melissa E Middeldorp, Kurt C Roberts-Thomson, et al. Pericardial fat is associated with atrial fibrillation severity and ablation outcome. *Journal of the American College of Cardiology*, 57(17): 1745–1751, 2011.